

# Characteristics of high-resolution sea ice dynamics in the Gulf of Finland, Baltic Sea

Madis-Jaak Lilover<sup>1,\*</sup>, Juss Pavelson<sup>1</sup>, Tarmo Kõuts<sup>1</sup> and Matti Leppäranta<sup>2</sup>

<sup>1)</sup> Tallinn University of Technology, Department of Marine Systems, Akadeemia 15A, EE-12618 Tallinn, Estonia (\*corresponding author's e-mail: madis.lilover@ttu.ee)

<sup>2)</sup> Institute of Atmospheric and Earth Sciences, P.O. Box 68, FI-00014 University of Helsinki, Finland

Received 3 Jan. 2018, final version received 19 Mar. 2018, accepted 4 May 2018

Lilover M.-J., Pavelson J., Kõuts T. & Leppäranta M. 2018: Characteristics of high-resolution sea ice dynamics in the Gulf of Finland, Baltic Sea. *Boreal Env. Res.* 23: 175–191.

High-resolution Eulerian and Lagrangian sea ice kinematics are examined based on an ADCP and four icebound drifting buoys in the Gulf of Finland, Baltic Sea. The measurements were performed in the central Gulf of Finland in winter 2010 from January to March. Ice drift was mostly in near-free drift state driven by winds and ice-independent currents in the basin. Internal friction was significant, apart from off-ice forcing toward the open boundary. The averaged asymptotic ice/wind speed ratio and deviation angle at higher wind speeds were 0.034 and 9° in the oceanic boundary layer, respectively. The ratio depended on the direction of the wind indicating the role of morphometry of the coast to the local ice kinematics. The maximum values of wind ratio were observed in cases of NE winds and minimum values in cases of SW winds. Coherent ice drift was observed up to a distance of 42 km.

## Introduction

A drifting sea ice field consists of a large number of ice floes and forms a granular medium. Forced by winds and ocean currents, each ice floe follows its own individual trajectory, while interacting at the same time with neighbouring ice floes. On scales much larger than the floe size, a continuum approximation is commonly assumed, resulting in a two-dimensional, compressible and non-linear continuous geophysical medium (e.g., Leppäranta 2011). Wind is regarded as an independent external force while the oceanic forcing depends on the velocity difference between ice and water. Tidal forcing is insignificant in the Baltic Sea. The response of drift ice to these external forces is dictated by its inertia, rheol-

ogy, and re-distribution of ice thickness field. In particular, in land-bounded floe fields with high ice concentration, interactions between ice floes create strong friction and can even prevent the ice from moving, while open floe fields are free from significant mutual interactions.

The physics of sea ice drift is fairly well understood (e.g., Hibler 1986, Leppäranta 2011, Weiss 2013) but there are still major open questions. Firstly, ice thickness redistribution question has been lacking for good data although it has a key role in sea ice modelling. Sea ice deformation changes the ice thickness field but it is not known in detail from observations and therefore quite simplistic approaches are employed in modelling. Secondly, dynamic ice–ocean interaction is usually parameterised with a

simple drag law, which shows large uncertainties at frequencies above the inertial (Coriolis) frequency (Leppäranta *et al.* 2012) and in the presence of non-neutral stratification. A major issue is the spatial and temporal scaling laws of sea ice dynamics, in particular thickness, velocity, strain, and stress. Temporal characteristics of ice drift have been investigated in papers presenting drifter data (e.g., Hibler *et al.* 1974, Ono 1978, Leppäranta 1981, Thorndike and Colony 1982, Leppäranta and Omstedt 1990, Schevchenko *et al.* 2004, Leppäranta *et al.* 2012), where the close connections of ice motion with wind and Coriolis and tidal forcing are recognised. Inertia of the ice itself shows up only on time scales less than one hour. At present, techniques exist to monitor ice velocity at very high accuracy and high temporal resolution (e.g., MacMahan *et al.* 2009).

Less work has been done on the spatial characteristics of ice drift and the present knowledge of spatial variability of ice motion is still only qualitative. Thorndike (1986) analysed Argos drift buoy data for spatial correlation structure in longitudinal (parallel to ice motion) and transverse drift directions, and Kheysin (1978), Sanderson (1988) and Richter-Menge *et al.* (2002) examined scaling of internal ice stress over spatial length scales. Overland *et al.* (1995), Goldstein *et al.* (2009) and Stern and Lindsay (2009) and Weiss (2013) all discuss spatial structures and scales in sea ice velocity field. Ryabchenko *et al.* (2010) modelled the dynamics of drifting sea ice in the Gulf of Finland and concluded that it plays an important role in the evolution of landfast ice zone in the eastern part of the Gulf.

A better knowledge of the time–space scaling question is required for research and applications (cf. e.g., Sanderson 1988, Leppäranta 2011, Weiss 2013). The spatial structure of ice thickness has been studied based on the traditional ice thickness distribution (Thorndike *et al.* 1975) but the time evolution is still a major issue. The best data have been provided by upward-looking submarine and moored sonars that have several limitations. Comparisons between sea ice velocities from model simulations and Radarsat data have shown that the present models are incapable of producing spatial or temporal scaling relations that match those observed in nature (e.g., Girard

2009, Leppäranta *et al.* 1998). The time co-ordinate presents a more straightforward modelling problem, as it can be approached using the continuum theory but in spatial scaling, one needs to go from a continuum dynamics to granular flow and further to interior dynamics of individual ice floes. Spatial scaling is very important for practical applications since it is connected to forces that can act on ships and fixed structures. Temporal scaling is connected to short-term (1 day) and very short term (1 hour) local forecasting problems in ship route planning, ice management related to oil platforms and combatting of oil spills, and evaluation of ice pressure in ice engineering.

The Gulf of Finland is seasonally ice-covered for 3–5 months. It has an elongated form — 330 km long and 80–100 km wide — and the main shipways are for tanker and cargo traffic along the longitudinal east–west axis and passenger ships across. The presence of ice cover sets special requirements for navigation, both for the construction of the ships and their behaviour in ice, as in many cases, merchant ships need icebreaker assistance. Therefore, the detailed knowledge about ice conditions and their variability is required. In particular, ice kinematics and dynamics have a substantial impact on navigation conditions by causing rapid changes in compressive forces, which act upon a ship's hull. Thus, the ice cover brings severe risks to the ship, with consequences to the economy and environment of the region.

In this work, sea ice kinematics data of high temporal resolution are analysed in the Gulf of Finland, in the Baltic Sea. The data were collected using the bottom-track facility of the ADCP (Acoustic Doppler Current Profiler) and icebound drifter buoys in the frame of the European Union (EU) FP7 project SAFEWIN (Safety of winter navigation in dynamic ice). Preliminary results based on the present data set were published by Kõuts *et al.* (2012) and Lilover *et al.* (2013). Still, the comprehensive study which combines Eulerian and Lagrangian high-resolution measurements (with temporal resolution 10 and 30 minutes, respectively) is missing for the Gulf of Finland as well as for other ice-covered regions of the Baltic Sea. In this paper, we focus on the description of sea ice kinematics in differ-

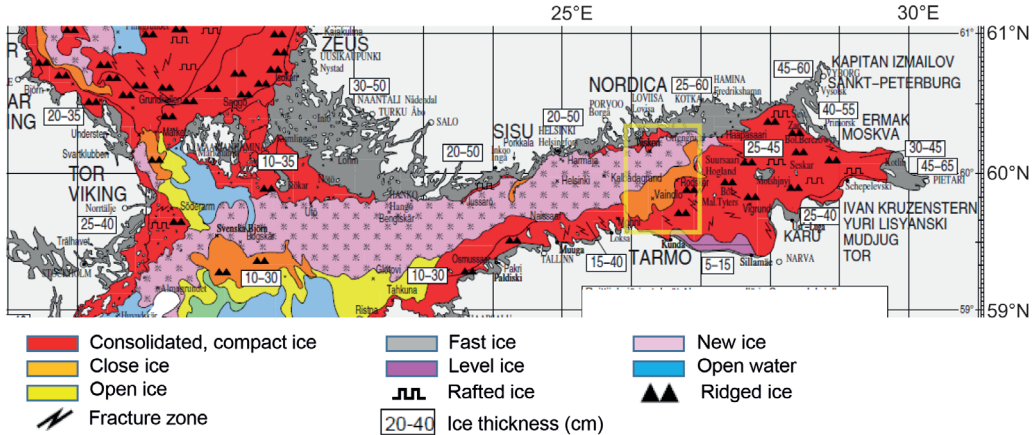


**Fig. 1.** Part of an ice chart of the Baltic Sea for 16 March 2010 (Finnish Meteorological Institute). Shallow area (less than about 10 m) approximately coincides with land fast ice zone. Measurement campaign area in March is marked by a yellow square.

ent time (from 10 min to 2 months) and spatial (from 1 km to 60 km) scales across the central part of the Gulf of Finland in relation to varying wind forcing.

## Material and methods

### Site

The Gulf of Finland is the eastern basin of the brackish Baltic Sea (Alenius *et al.* 1998, Soomere *et al.* 2008). Its size is about 330 × 90 km and its mean depth is 37 m. The basin freezes to a greater or lesser extent every winter, starting from the colder, shallower and less saline eastern part (Fig. 1). Mean ice thickness varies depending on the severity of the winter. The level ice thickness is typically 30–50 cm. The geometry of the basin has a considerable influence on the ice types. The main ice type is drift ice, landfast ice only forms in limited areas along the coast landward from the 10 m isobath (Leppäranta 1981). The basin is large enough for the wind forcing to overcome the ice strength, so that ice ridges are formed during strong wind events (Leppäranta 1981, Uotila 2001). Ridges are typically up to 5–15 m thick (Leppäranta and Hakala 1992). The wind pattern is not uniform across the basin because of its elongated shape, which creates a kind of ‘wind tunnel’ (Soomere 2003). The size of the basin is relatively small

compared to the typical scale of atmospheric low-pressure systems. Hence, pressure and compressive ridges are primarily formed on the windward side of the basin and leads are formed on the leeward side.

In the Baltic Sea, sea ice drift is mainly forced by wind and in cases of long fetches from the west wind builds up major stresses. Since the Gulf of Finland is strongly elongated, westerlies produce the most intensive compressive situations, also in severe winters easterly winds may form high stresses near the northern coast. In the south, the sea area off Kunda in the middle of the basin is known as an area of severe ice conditions because of heavily ridged ice around small islands and in shallow areas. This area was selected for measurements of local high-resolution sea ice kinematics by ADCP.

### Sea ice dynamics

Sea ice drift is forced by winds and currents and resisted by ice–water drag and internal friction of the ice (e.g., Leppäranta 2011). The fundamental equations are the conservation laws of momentum and ice, respectively,

$$\rho h \left( \frac{\partial \mathbf{u}}{\partial t} + \mathbf{u} \cdot \nabla \mathbf{u} + f \mathbf{k} \times \mathbf{u} \right) = \nabla \cdot \boldsymbol{\sigma} + \boldsymbol{\tau}_a + \boldsymbol{\tau}_w - \rho h \nabla \zeta \quad (1a)$$

$$\frac{\partial h \mathbf{u}}{\partial t} = \nabla \cdot (h \mathbf{u}) \quad (1b)$$

where  $\rho$  is ice density,  $h$  is mean ice thickness,  $\mathbf{u}$  is ice velocity,  $t$  is time,  $f$  is Coriolis parameter,  $\mathbf{k}$  is unit vector vertically upward,  $\boldsymbol{\sigma}$  is internal ice stress,  $\boldsymbol{\tau}_a$  and  $\boldsymbol{\tau}_w$  are shear stresses of air and water on the top and bottom surfaces of ice, respectively, and  $\zeta$  is sea level elevation. The shear stresses  $\boldsymbol{\tau}_a$  and  $\boldsymbol{\tau}_w$  are expressed using quadratic drag laws as

$$\boldsymbol{\tau}_a = \rho_a C_a |\mathbf{U}_a| \mathbf{U}_a \quad (2a)$$

$$\boldsymbol{\tau}_w = \rho_w C_w |\mathbf{U}_w - \mathbf{u}| (\cos\theta_w + k \times \sin\theta_w) (\mathbf{U}_w - \mathbf{u}) \quad (2b)$$

where  $\rho_a$  and  $\rho_w$  are the densities of air and water,  $C_a$  and  $C_w$  are the drag coefficients of air and water,  $\mathbf{U}_a$  is surface wind velocity,  $\mathbf{U}_w$  is current velocity, and  $\theta_w$  is the corresponding turning angle under the ice. Internal stress is normally decomposed into the form  $\boldsymbol{\sigma} = P(A, h)\Gamma(\dot{\epsilon})$ , where  $P$  is ice strength,  $A$  is ice compactness and  $\Gamma$  is a tensor function of the strain-rate  $\dot{\epsilon}$ .

The governing forces on the ice in the Gulf of Finland are the air and water shear stresses and the internal friction. The free drift model assumes that the internal friction is zero. Then the balance of the air and water stresses and Coriolis term provides the solution

$$\mathbf{u}_w = \mathbf{u}_a + \mathbf{U}_w, \mathbf{u}_a = \alpha (\cos\theta + k \times \sin\theta) \mathbf{U}_a \quad (3)$$

Asymptotically for  $\frac{U_a}{hf} \rightarrow \infty$ :  $\alpha \rightarrow \sqrt{\frac{\rho_a C_a}{\rho_w C_w}}$ ,  $\theta \rightarrow \theta_w$

where  $\mathbf{u}_a$  is wind-driven ice drift, with a speed 2%–3% of wind speed, depending mainly on the drag coefficients. In the presence of strong internal friction, ice velocity is smaller. At the extreme, for plastic rheology, even in the presence of nonzero external forcing we may have  $\mathbf{u} \equiv 0$ . Plastic flow begins when forcing reaches the yield strength. In the one-dimensional case, the quasi steady-state solution is obtained from

$$(u - U_w)^2 = \frac{\rho_a C_a}{\rho_w C_w} U_a^2 - \frac{d}{dx} \left( \frac{P}{\rho_w C_w} \right) \quad (4)$$

When the ice is moving toward a fixed boundary, a strength gradient exists to reduce the velocity from the free drift value. When ice drifts eastward in the Gulf of Finland and becomes more and more densely packed, the velocity slows down from the free drift to zero.

## Sea ice velocity spectra

Free drift follows the linear model, where the solution is the superposition of wind-driven drift and geostrophic current. In addition, there is also a random component due to the variable size and shape of ice floes. Assuming these forcing factors to be independent, their spectra  $p_a$ ,  $p_w$  and  $p_s$ , respectively, can be superposed for the ice velocity spectrum:

$$\alpha = \frac{\lambda_i^2 + f^2 + \omega^2}{\left[ (\lambda_i + \lambda_w)^2 + (\omega + f)^2 \right] (\omega + f)^2} \quad (5)$$

$$\lambda_i = \frac{\rho_w C_{w1}}{\rho_i h}, \lambda_w = \frac{C_{w1}}{D}$$

where  $\omega$  is frequency,  $\alpha$  is the spectral wind factor,  $\lambda_i$  and  $\lambda_w$  are the ice and water inverse dynamic time scales, respectively,  $C_{w1} \sim 0.3 \text{ cm s}^{-1}$  is the linear ice–water friction coefficient and  $D$  is the depth of the Ekman layer. At very low frequencies,  $\alpha \sim 0.6 \times 10^{-3}$  is a constant and at very high frequencies  $\alpha$  falls as  $\omega^{-2}$ . Since  $\lambda_i \gg \lambda_w, f$ , these low- and high-frequency limits come at  $\omega_1 < \lambda_w, f \sim 10^{-4} \text{ s}^{-1}$  and  $\omega_2 > \lambda_i \sim 10^{-2} \text{ s}^{-1}$ , respectively. The corresponding cycle periods are 14 hours and 10 minutes, respectively. There is not much known about the random component as the study of this topic needs a very high time-space measurement accuracy.

The free drift contains the “forcing components” by the wind and current spectra, the dominance of which may vary. In a purely wind-driven case, the outcome consists of power law  $\propto \omega^{-p}$  and an inertial peak at the frequency of  $-f$ . The power follows the turbulent spectrum of wind until very high frequencies and then falling faster. In the presence of internal friction, the spectrum is damped. For small effects, damping is independent of frequency, and in the extreme case the ice is stationary (i.e., there is no kinetic energy) (Leppäranta 2011). There is also a difference if the data used for calculations are Eulerian or Lagrangian. In the Eulerian case, the random component comes from different ice floes passing a fixed point in space, alternatively, in Lagrangian case, the drifter is on a fixed ice floe and random movements may come from floe rotations due to variable forcing (cf. Leppäranta 2011).

## Data sources

Earlier publications relying on present data set treated single topics like (1) ice cover periods at ADCP site, (2) sea ice drift speed versus wind speed and (3) trajectories of icebound drifter data but didn't compose drifters and ADCP data to illuminate sea ice drift dependence from wind in time and in space (Kõuts *et al.* 2012, Lilover *et al.* 2013).

The present dataset consists of ice speed data collected by bottom-mounted ADCP and drifting buoys. Winter 2010 was colder than an average, and the whole Gulf of Finland froze over (Fig. 1). Near the southern coast, the ice conditions were quite variable due to south-westerly winds occasionally producing large open water areas. The main study area was selected as the section between Kotka, Finland and Kunda, Estonia, almost a north–south section between the longitudes 26° and 27°E (Fig. 1). The satellite data used are Synthetic Aperture Radar data from RADARSAT-2 and Envisat (SEAICE\_BAL\_SEAICE\_L4\_NRT\_OBSERVATIONS\_011\_004 <http://marine.copernicus.eu>) to describe ice concentration and visual data from MODIS (Moderate resolution imaging spectrometer of Aqua/Terra satellite of NASA) to describe evolution of spatial changes of ice cover. MODIS images of the ice conditions at the instrument sites are shown in Fig. 2. At the end of February, the southern side of the Gulf of Finland was ice-free. After a strong NW wind event in March, the ice including the drifting buoys drifted massively to the east.

The ADCP was deployed in the central zone of the Gulf of Finland on 12 January 2010 and recovered on 27 April 2010. The site (59°42.09'N, 26°24.23'E, depth 63 m) was located in the deep basin extending south–east toward Kunda Bay, around 15 km from the coast (Fig. 2). Bottom-mounted upward-looking ADCP has been successfully used for a couple of decades at different depths and in different seas. The primary purpose of ADCP sounding is to measure the vertical profiles of currents, but there are also studies for the monitoring of ice kinematics (Belliveau *et al.* 1990, Visbeck and Fischer 1995, Strass 1998, Shcherbina *et al.* 2005). Björk *et al.* (2008) used this method in the Baltic Sea. In this paper, the

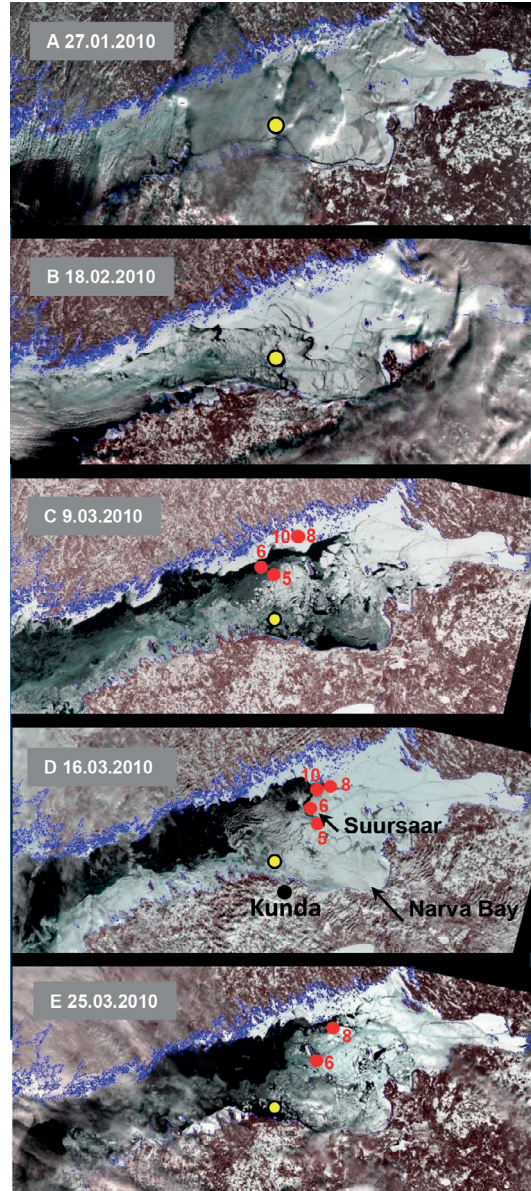


**Fig. 2.** MODIS images of the ice conditions in the Gulf of Finland on 27 January 2010, 18 February 2010, prior to the installation of the drifter buoys, and on 9, 16 and 25 March 2010 corresponding to the ADCP ice-covered periods A, B, C, D and E (images from NASA, processed by Dr. Liis Sipelgas). The drifters are named by numbers 5, 6, 8 and 10, and their positions are marked with red dots, the ADCP location is marked with a yellow dot. Key names of locations are given in panel D.

data of a recent measurement campaign conducted in the Gulf of Finland in winter 2010 as part of the EU FP7 project SAFEWIN are analysed. In the

frame of that campaign, a 307.2 kHz broadband ADCP (Workhorse Sentinel, RD Instruments) was deployed on the bottom with a trawl-resistant Barnacle 60P platform. The bottom-track (BT) option of the ADCP with a sampling interval of 10 minutes (an average of five high-frequency pings) was utilised to trace from below the sea surface/ice bottom. The data include ice drift velocity (its BT velocity), BT error velocity and the actual depth (the distance from the instrument's head to the sea surface/ice bottom). The BT velocities have a single-ping accuracy of a few  $\text{mm s}^{-1}$  and the depth resolution is approximately 0.1 m. The ice velocity was estimated with an accuracy of  $0.5 \text{ cm s}^{-1}$ . The four-beam geometry of the ADCP allows two independent vertical velocities to be computed. The difference between these velocities determines the BT error velocity. Wave motions in open water give different vertical motion for each beam and therefore large error velocity. If the flow field is homogeneous, the difference will average out to zero. Björk *et al.* (2008) found that open water increases the variance of the error velocity by a factor of three. BT error velocity is therefore used to discriminate situations with open water from those with ice coverage.

Generally, the data records were continuous, but specific short gaps were detected during both the ice formation phase (approximately one week in January) and the ice break-up stage (nearly three weeks in March). While the data quality of the rest of the measurement series was good, we attribute the missing data to distorted backscattering of acoustic signals from unstable new ice formations — like frazil, brash ice and slush — while the ice was forming. During the break-up, the rising temperature and sunlight caused the ice porosity to increase with pores filled with seawater. Thus, the density of the melting ice layer became very close to seawater density, which probably also caused distorted backscattering of the acoustic signal.

BT velocity series with resolution in time of 10 minutes were first filtered with a simple 2-hour moving average filter and then decimated to obtain hourly values for further analysis. The same procedure was applied to the time-series of wind speed. For low-frequency analysis, all data series were filtered with a 36-hour moving average filter. Such a low-pass filter window was

chosen to remove inertial oscillations (period: 13.9 hours), tides and seiche-driven oscillations, with the longest periods in the Gulf of Finland around 31 hours (Alenius *et al.* 1998). As an exception for spectral analysis, time series with a resolution of 10 minutes were used.

Four drifters were deployed during the R/V *Aranda* cruise in the Gulf of Finland in March 2010. The ice drifter experiments lasted for a total of 66 days, from 8 March to 14 May. The drifters were launched in two groups: drifters 5 and 6 in the middle of the gulf about 15 nautical miles north of the ADCP station, with a maximum distance between buoys about two nautical miles; drifters 8 and 10 were launched even further to the north, around 32 nautical miles from the ADCP station. The drifters are compact, about 1 m long, with a diameter of 11 cm and mass of 10 kg, developed by a local engineering company. Their measurement interval can be controlled remotely between 15 minutes and 2 hours during field experiments. Data are transmitted in real time via GSM networks, using a GPRS protocol, if a cellular service is available (otherwise the data are stored on a memory card and transmitted once GSM connection has been reached). Thus, even if a drifter is lost from real-time monitoring, the data can still be retrieved.

A summary of the drifter experiment is given in Table 1. In this table, UTC is used, local wintertime is UTC + 2 hours, which is about 15 minutes ahead of the solar time. Data of the wind speed and direction were obtained from the meteorological station in Vaindloo Island ( $59^{\circ}49.66'N$ ,  $26^{\circ}21.60'E$ ), thirteen kilometres north of the ADCP site. The measurement altitude was 32 m and the data were stored at 5-minute intervals, in neutral atmospheric stratification, the wind speed at this altitude is 11.5% higher than the standard surface wind at the 10-m altitude, based on the roughness length of 0.04 cm of Baltic Sea ice (Joffe 1982).

## Results and discussion

### Ice cover periods derived from ADCP and MODIS data

In winter 2010, ice cover of the Gulf of Finland

was very dynamic and landfast ice formed only in the coastal zone. Ice conditions were highly dependent on the wind regime. Westerly winds pushed the ice further east as far as the strength of ice allowed. In the east, it resulted in a relatively stable, compact ice cover with a ridged ice zone, which could be almost as stable as landfast ice. One area of compacted drift ice was observed near the ADCP site off Kunda, nearby the Uhtju islands. These small islands restricted eastward-moving ice mass forming heavy ridges, which then froze together into a stable ice cover. A north-westerly wind is the most favourable for pushing ice formed near the Finnish coast towards Kunda. Due to low tensile strength of drift ice, southerly winds can still fracture the ice and transport it northward back to the Finnish coast. This was relatively easy in winter 2010, as there was frequently open water or new ice on the Finnish side. The changing wind forcing caused periods of changing ice and open water in our study area. The leads seen in Fig. 2 near the north and south coasts of the Gulf of Finland caused the fast alternation of ice regimes at our ADCP mooring site. The characteristics of leads and their importance to ship traffic are thoroughly discussed for the region in Pärn and Haapala (2011).

In an ice-covered basin with intense ship traffic such as the Gulf of Finland, one would anticipate that the breaking of ice by ships has an influence on sea ice dynamics. Ice cutting could affect the mobility of the ice and diffusion of ice floes. However, there has been so far no research work on this question. In our case, the data do

not give possibilities to examine the role of ships in sea ice mechanics directly, but from MODIS images it appears that shipping tracks played a minor role in comparison of natural leads in the Gulf of Finland.

The bottom-mounted ADCP BT error velocity time-series are analysed to distinguish periods of ice cover and open water during the measurement period. The discovered longer and more stable ice periods are marked with the letters A, B, C, D, and E (Table 2). The periods C, D and E coincide with drift buoy measurements. The correspondence of low variance of error velocity to ice-covered periods and high variance to ice-free periods were validated using MODIS satellite imagery. In Fig. 3, the circles mark the dates when ice was observed in the area and the dots when ice was not observed (corresponding mean standard deviations are given below the upper edge of the figure). The standard deviations of BT error velocity within the ice cover periods were 3–5 times smaller than in open water conditions. Different ice situations according to the MODIS imagery are presented in Fig. 2 for ice cover periods C, D and E, showing that ice conditions were highly variable in the Gulf of Finland during the period of our study.

## General characteristics of ice dynamics

Because of its elongated shape and fixed boundary in the east, besides of ice concentration and thickness, the wind characteristics (speed, direction, and durability (persistence)) determines the

**Table 1.** Drifter experiment in the Gulf of Finland in winter 2010. Average drift speed is an averaged value of successive drift speeds (the values affected by gaps in measurements were excluded).

Drifter	Date and time (UTC) of start and end	Lat. N	Long. E	Distance from launching point (km)	Length of drift path (km)	Drifting period (days)	Average drift speed (m s <sup>-1</sup> )
5	8 Mar 16:46	59°56.92′	26°09.14′	46.8	79.6	7.13	0.09
	15 Mar 20:00	59°52.20′	26°58.77′				
6	8 Mar 17:30	59°58.75′	26°01.32′	68.2	559.7	66.57	0.11
	14 May 07:18	60°23.22′	26°56.38′				
8	8 Mar 17:30	60°14.76′	26°38.29′	87.8	447.9	60.56	0.08
	14 May 07:18	60°30.81′	28°07.54′				
10	8 Mar 17:30	60°14.75′	26°38.28′	66.1	233.6	43.24	0.08
	14 May 07:18	60°16.87′	27°49.59′				

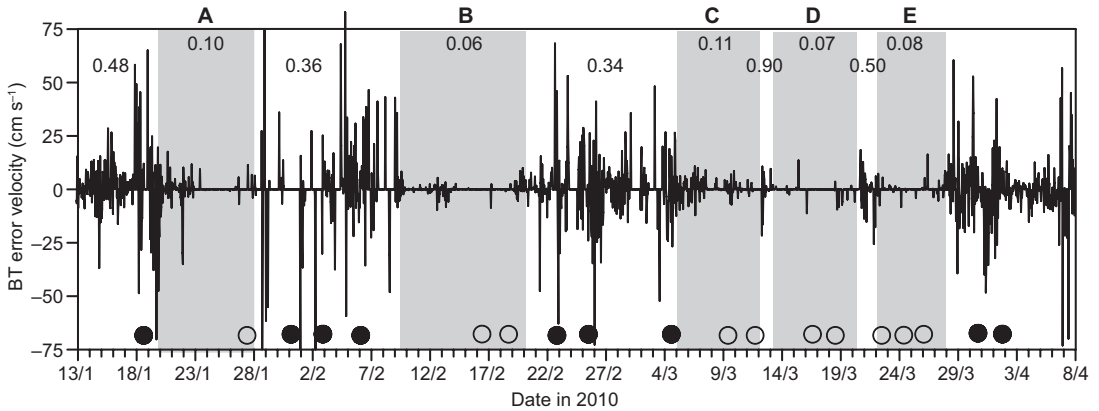


**Fig. 3.** Bottom-track error velocity during the observation period (redrawn from Kõuts *et al.* 2012). Shaded areas with labels A, B, C, D, and E show the periods where ice was detected above the ADCP. The timing of available cloud-free MODIS images confirming the ice (circles) and open water (dots) at the measurement site is shown above the x-axis.

ice drift speed in the Gulf of Finland. When wind is pushing ice toward the open (western) boundary, the high ice drift speed can be observed, in reversed case westerlies push ice toward the eastern fixed boundary and lower ice drift speeds are expected. The drift toward north or south is more limited due to the narrow geometry of the basin. The ADCP ice velocity histograms are shown in Fig. 4 for periods A–E. The frequent occurrence of ice velocities close to zero (ice speed from 0 to 2 cm s<sup>-1</sup>) points to the Gulf of Finland shoreline (and associated internal friction) effect on the ice drift speed. In the cases when the wind was pushing ice toward the eastern or northeastern boundary, the highest occurrence of “zero” ice drift speed was observed (Fig. 4f).

The ice cover area calculated on the basis of sea ice concentration data for the Gulf of Finland showed local maxima at observed ADCP ice cover periods A–E, whereby the most prominent “zero” speed events dates coincided with ice-covered area peak values (Fig. 5). In most

cases when the “zero” ice speed was observed, a continuous, notable forcing was on by the wind. For example, in case of sub-period D (having the largest “zero” ice speed occurrence), the wind was pushing ice eastward until it stopped moving at second half of 15 March (Fig. 6).

The only explanation is that the plastic internal friction of ice played an important role since the “zero” ice speed occurrence showed such peak. For described “zero” ice speed case the maximum wind speed was 6 m s<sup>-1</sup> giving the compressive strength of ice ( $P^*$ ) of at least 16 kPa [for fetch  $L = 100$  km and ice thickness  $h = 0.5$  m, the yield criterion  $\tau_{\alpha}L > Ph$  was used (Leppäranta 2005)]. Ice started to move again at the second half of 18 March when the wind direction changed pushing ice toward the north. A similar relationship with the wind was observed for ice cover periods B and E, the ice stopped moving when ice cover was pushed eastward and ice began to move when the wind changed direction. In the case A, ice stopped

**Table 2.** Ice drift characteristics at ADCP site.

Ice period	Date in 2010	Drifting period (days)	Averaged drift speed (m s <sup>-1</sup> )	Maximum drift speed (m s <sup>-1</sup> )	Asymptotic wind factor	Asymptotic deviation angle
A	20–28 Jan	7.875	0.18	0.5	0.037	15°
B	9–20 Feb	11.375	0.24	0.83	0.040	3°
C	5–11 Mar	5.55	0.27	0.88	0.028	15°
D	13–20 Mar	8.0	0.09	0.88	0.037	7°
E	22–27 Mar	4.7	0.15	1.01	0.029	5°

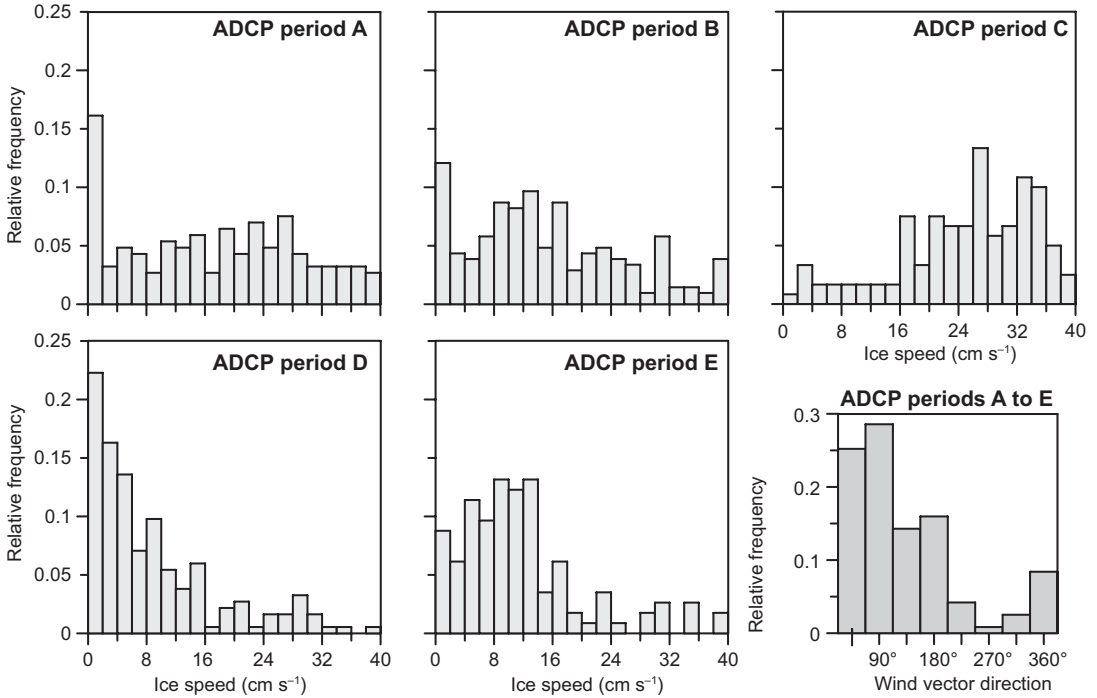


**Fig. 4.** (a–e) Histograms of observed ice velocities (measured by the ADCP) for time periods A–E, indicated in Table 2, (f) the occurrence of “zero” ice speed according to wind vector direction at ADCP site all periods total. To the measured wind direction was added 180° to get the wind vector (wind forcing) direction.

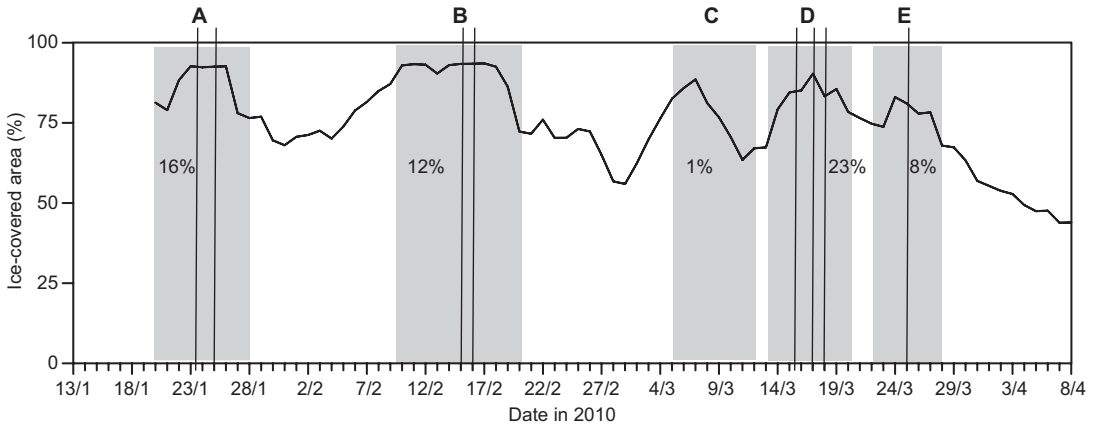


**Fig. 5.** Ice-covered area in the Gulf of Finland in winter 2010 (sea ice concentration data provided for processing by E.U. Copernicus Marine Service Information, processed by Dr. Ove Pärn). Shaded areas with labels A, B, C, D and E show the ice cover periods at the ADCP site position. The thin vertical lines mark the (near-)zero drift speed events with the percentage numbers for the zero ice speed frequencies.

moving in both northward and southward winds, but similar to other sub-periods it started to move when the wind direction changed.

According to the drifters, the most prominent movement of the ice occurred between 10 and 13 March, when strong southwesterly and

northwesterly winds (maximum wind speed was 19 m s<sup>-1</sup>) pushed most of the ice mass from the northern coast of the Gulf of Finland toward southeast, to Suursaar [Gogland] and Narva Bay. This event is illustrated in Fig. 2, where the initial positions of the buoys (C) and their sites after

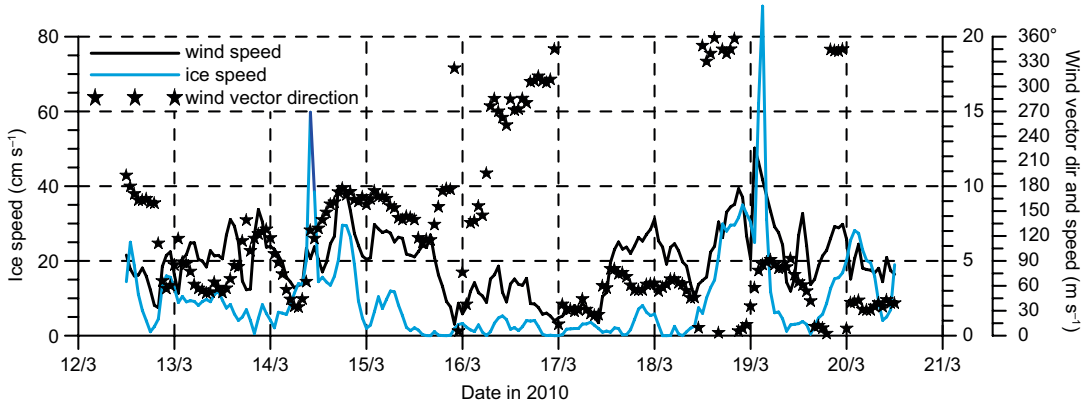


**Fig. 6.** Ice speed in relation to wind vector direction and speed for period D. The measured wind direction was turned by 180° to match the wind forcing with the current direction. Ice speed is marked by a blue line, wind speed by a black line and wind vector direction by stars.

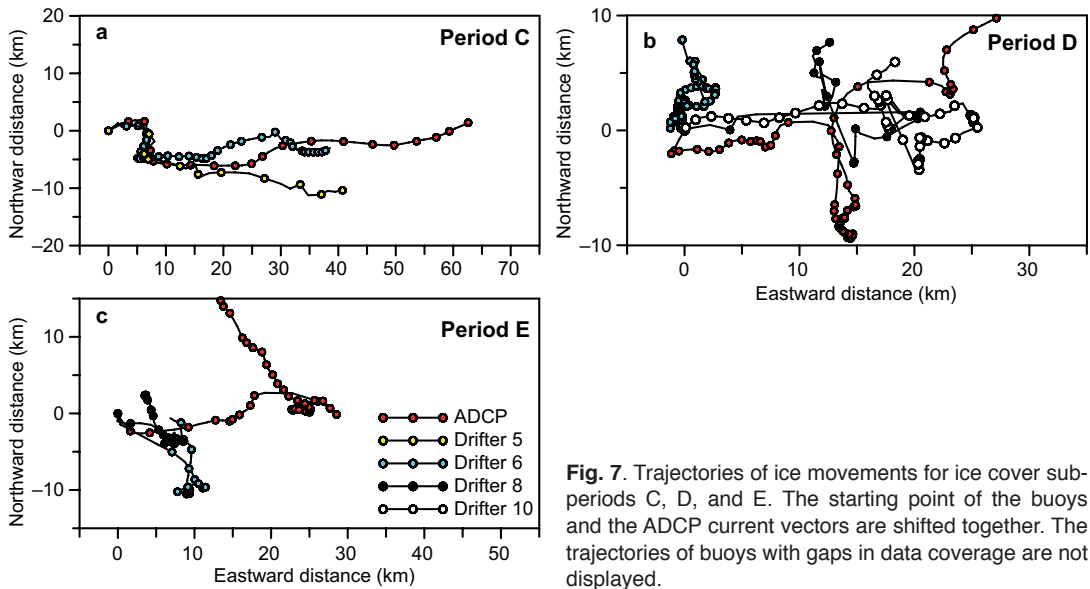


**Fig. 7.** Trajectories of ice movements for ice cover sub-periods C, D, and E. The starting point of the buoys and the ADCP current vectors are shifted together. The trajectories of buoys with gaps in data coverage are not displayed.

the storm (D) are shown. The drifters recorded the highest drift speeds for the entire measurement period, up to  $0.7 \text{ m s}^{-1}$ , during this event. Thereafter, speeds rarely reached  $0.3 \text{ m s}^{-1}$ , posting an average of about  $0.1 \text{ m s}^{-1}$  (Table 1). The maximum speeds were at the highest level reported in the Baltic Sea drifter experiments (cf. e.g., Leppäranta 1981, Leppäranta *et al.* 2001). In Bothnian Bay by an ADCP the maximum ice speed about  $0.5 \text{ m s}^{-1}$  was recorded (Björk *et al.* 2008). In theory, the maximum ice speed would be around  $1.25 \text{ m s}^{-1}$  in the Baltic Sea, with wind speed of  $25 \text{ m s}^{-1}$  driving the ice to the speed of

$0.75 \text{ m s}^{-1}$  and current velocity possibly adding a maximum of  $0.5 \text{ m s}^{-1}$  to that.

Ice drift variability across the gulf was described comparing the trajectories deduced from the ADCP ice drift measurements and the trajectories of the drifting buoys (Fig. 7). During ice period C, the drifters 5 and 6 and ice at ADCP site drifted almost coherently (Fig. 7a). However, closer to the southern coast (ADCP site) the ice drift speed was higher than in the middle of the basin. Period D was characterized by more heterogeneous drift across the basin. The ice in the middle of the gulf (drifter 6) was

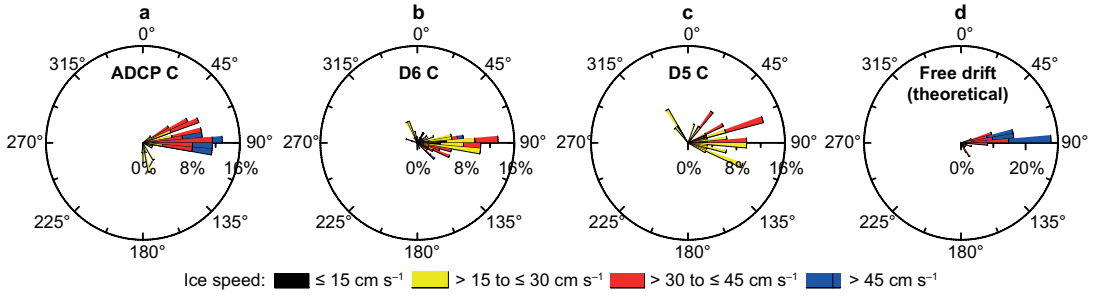


**Fig. 8.** Ice drift velocity roses for sub-period C (a) ADCP-measured ice drift direction and ice drift speed, (b) buoy 6 drift direction and drift speed, (c) buoy 5 drift direction and drift speed and (d) the theoretical wind-driven free ice drift direction and speed are given for comparison. Colour scales are shown in the bottom of the figure.

barely moving (or was in a circular motion), while in the north and south the ice drift had similar velocities and at times similar behaviour (like north-eastward movement at the end of the period). During period E, the ADCP data and drifter data had a similar pattern but with generally higher velocity at the ADCP site. The observed drifter tracks which basically follow the wind forcing differ by ice drift speed across the Gulf of Finland probably due to different ice compactness (the presence of leads either close to the southern or northern coast). For example, in case of sub-period C the drifter 6 speed in vicinity of northern lead reached 70% of ADCP site ice speed (located close to the southern lead) while outside of the northern lead region (sub-period E) the drifter speed reached only to 50% of ADCP site ice speed (Fig. 2). Thus, the leads enable the high mobility of ice in a changing wind field. The directional distribution of ice drift also indicated the role of leads — namely the ice drift polar histograms for period C showed that the northern drifter D6 (located close to the lead area, Fig. 2) had less scattering of drift angle compared to the drifter D5 and ADCP site (Fig. 8) probably because of less internal friction of ice there. The theoretical wind-driven free ice drift (deduced from wind data using wind factor 0.03 and 20° deviation to the right with respect to the wind vector) shows least scattering (internal friction has been not counted) (Fig. 8d).

The scatter-plots of the hourly ice-drift and winds speeds (Kõuts *et al.* 2012) revealed a clear relationship between the ice drift speed and the wind speed during the ice sub-periods A–E, but

the character of the relationships still varied between them and even within the one sub-period. The best-fit wind factor ranged in 2%–4%, but the scatter was large. An analysis of low-pass-filtered data (periods less than 36 hours removed) during sub-period C, actually showed two different ice speed vs. wind speed relationships that could be a result of the influence of ocean currents or internal friction of ice or concurrently both (Fig. 9). The sub-periods (A, B, D and E) did not reveal similar features. Differently from other periods, during sub-period C the wind pushed ice toward eastern shore (higher internal friction, current slightly against the ice drift direction) and out toward the open boundary (lower internal friction, current confluent with ice drift). Consequently, the ice drift responded to the forcing factors and resulted in two different ice/wind speed relations in the scatter plot (Fig. 9).

Equation 3 shows that in free drift the slopes of the lines should be the same and that the intercept on the  $y$ -axis gives the mean ice-driving current. In the presence of internal friction, the relation has a square root shape with the intercept of  $x$ -axis at

$$U_a = \sqrt{-\frac{1}{\rho_a C_a} \frac{dP}{dx}}$$

and the slope asymptotically approaching the free drift slope (Eq. 4). The internal friction shows in the lower envelope of the scatterplot intercepting wind axis at  $U_a \approx 3 \text{ m s}^{-1}$ , corresponding to the wind stress of 0.02 Pa. For this to scale with plastic yield strength  $P$  (cf. Eq. 4), we must have  $P \sim \tau_a \ell$ , where  $\ell$  is the fetch. Therefore, with  $H \sim 0.5 \text{ m}$  and  $\ell \sim 50 \text{ km}$ , we have  $P \sim 2 \text{ kPa}$ . This value

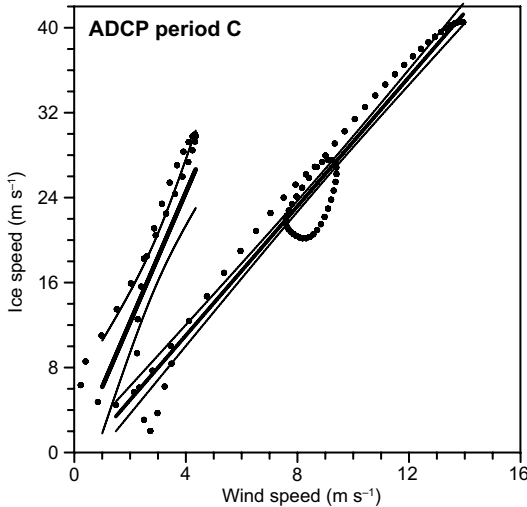


**Fig. 9.** Scatter-plot of the low-pass-filtered (for clarity the fluctuations of current and wind speeds with periods less than 36 hours are removed) ice drift and wind speeds for ice period C. The dashed line is the linear fit for the outward of the gulf ice drift phase and the bold line for into the gulf (eastward) ice drift phase. The thin lines mark 95% confidence limits.

is low, reflecting the high mobility of the present ice field due to ice compactness being significantly lower than 1. The yield strength decreases by one order of magnitude with compactness decreasing from 1 to 0.8–0.9.

The correlations between the wind and ice drift vectors, estimated via the method introduced by Kundu (1976), were very high: on an average 0.85 (Kõuts *et al.* 2012). By applying a linear fit for high wind speed and corresponding wind factor or deviation angle data (wind speeds higher or equal than  $10 \text{ m s}^{-1}$  were taken into account), the asymptotic values of wind factor and deviation angle were found. Namely, a linear fit value corresponding to the highest measured wind speed was taken for an asymptotic value. The ice-covered periods A, B, C, D and E revealed, based on hourly mean data, that the wind factor was in the range 0.028–0.040, giving an average of 0.034 (Table 2). These values are in accordance with earlier estimates. Typically, the wind factor can vary between 0.02 and 0.035, depending on the roughness of the ice: the low value represents a smooth ice surface and a higher value deformed ice cover (Leppäranta 2011). For comparison, Björk *et al.* (2008) estimated an

ice/wind speed ratio of 0.03 in the northern part of the Bothnian Bay. As shown by Eq. 3, the asymptotic values of the wind factor and deviation angle give information on the boundary-layer parameters. The asymptotic wind factor 0.034 provides the estimate of 0.92 for the ratio  $C_a/C_w$ . The air–ice drag coefficient is much better known than the ice–water drag coefficient and with  $C_a = 1.6 \times 10^{-3}$  (Joffre 1982) we have the estimate  $C_w = 1.7 \times 10^{-3}$ . This estimate is, however, lower by 50% than estimated earlier for the Baltic Sea ice fields (Leppäranta and Omstedt 1990). The asymptotic deviation angle  $\theta = 9^\circ$  is equal to the Ekman angle in the marine boundary layer. Typically, the angle value is  $30^\circ$  in the case of free ice drift in the Arctic (Thorndike and Colony 1982) and  $20^\circ$  in the case of thinner ice in the Baltic Sea (Leppäranta and Omstedt 1990). Similar measurements made in the Bothnian Bay produced a turning angle of ice drift compared to wind direction of around  $10^\circ$  (Björk *et al.* 2008).

As the dimensions of the Gulf of Finland — especially its width — are not large, free drift is likely to last only very short, and most of the time the morphometry of the coast plays a major role in the local ice dynamics. In winter, when southwesterly winds dominate, the current in the offshore areas is frequently observed to be against the wind (Lips *et al.* 2017) and could reduce the wind factor. Our measurements at ADCP location (summing up cases A to E and subtracting “zero” velocities) showed that in the cases when the wind was pushing ice toward west (sector between  $180^\circ$  and  $337.5^\circ$ ) the wind factor was above the average (3.5%) and when the wind was pushing ice toward east (sector between  $337.5^\circ$  and  $180^\circ$ ) below the average (Fig. 10). The maximum values of wind factor were observed when the wind was pushing ice toward the sector between  $180^\circ$  and  $225^\circ$  and minimum values for the sector between  $45^\circ$  and  $112.5^\circ$ .

### Temporal characteristics of ice drift

For a more detailed analysis of the ice velocity time series, we can examine the spectral properties.

The resulting Eulerian spectrum (Fig. 11) resembles the shape of the theoretical linear free

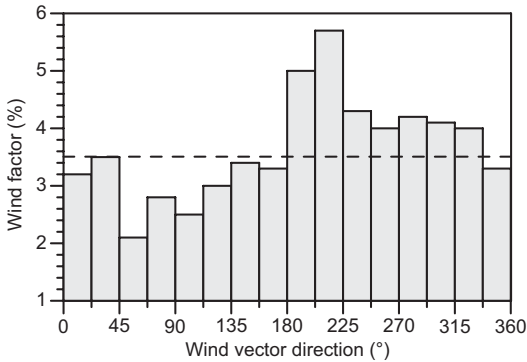


**Fig. 10.** Wind factor dependence from wind vector direction at ADCP site in periods A–E. To the measured wind direction was added  $180^\circ$  to get the wind vector (wind forcing) direction. The dashed line shows the mean value.

drift spectrum (Leppäranta *et al.* 2012, Fig. 2) which slopes above the time scale of ice inertia (1 hour) with the slope  $-5/3$  following the spectrum of the forcing. Asymptotically at very high frequencies, the slope steepens. The low-frequency level is at  $0.1 \text{ (m s}^{-1}\text{)}^2 \text{ cph}^{-1}$ . An inertial (Coriolis) signal shows up in the CW spectrum, as it should in theory, yet there is no sharp peak. The slope is  $-1.8$  in the frequency range of  $0.2\text{--}3 \text{ cph}$  for both counter-clockwise (CCW) and CW spectra. Taking the measurement error as a random term with an accuracy of  $\pm 1 \text{ cm s}^{-1}$ , the resulting spectrum is white noise at the level of  $0.67 \times 10^{-4} \text{ (m s}^{-1}\text{)}^2 \text{ cph}^{-1}$ . Ice velocity spectra reach this level at the frequency of about 3 cph.

The Lagrangian spectra produced from the drifter data are given in Fig. 12. The spectra could be estimated up to 0.25 cph. Their shape was similar to the Eulerian spectrum (Fig. 11) — namely, an inertial signal shows up in the CW spectrum, the spectral slope was close to  $-5/3$  in the frequency range  $0.03\text{--}0.25 \text{ cph}$  for CW spectra.

Eulerian and Lagrangian CCW spectra had roughly the same energy density values, but the Lagrangian CW spectra level was lower in the range  $0.04\text{--}0.2 \text{ cph}$ . This could be due to interactions between ice floes. In the Eulerian case, floes with random size and shape passed the site, while in the Lagrangian case we followed a fixed individual floe. Therefore, in Eq. 5 the noise term is expected to be larger than in the Eulerian case. The difference must, in general,

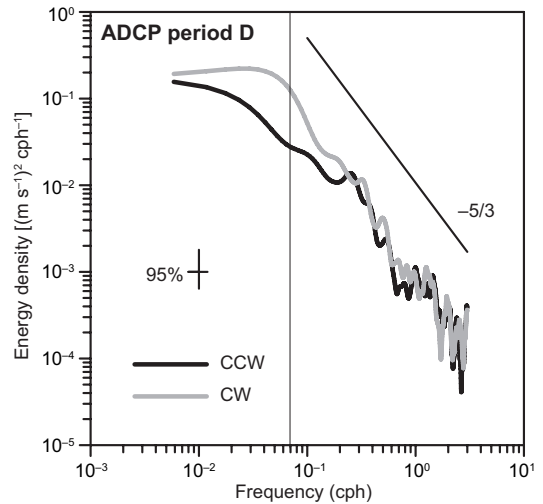


**Fig. 11.** Ice velocity spectra in period D at the ADCP site. CW is for clockwise and CCW for counter-clockwise frequencies. The thin vertical line marks inertial frequency (corresponds to local inertial period 13.9 hours). The inclined solid line refers to spectral slope  $-5/3$ .

depend on freedom of movement of individual floes and therefore on ice compactness and the floe distribution.

### Spatial characteristics of ice dynamics

The concurrent measurements of ice drift at the ADCP site and by drifters allow us to argue about the ice velocity length scales. The drifters were located in an area of  $10^4 \text{ km}^2$  and their distances to the ADCP site were  $33\text{--}60 \text{ km}$  (Table 3). The strength of the spatial correlation  $r$  of ice velocity depends on the length scale  $L$ , formulated as a power law as:

$$r(L) = a \left( \frac{L}{L^*} \right)^{-b} \quad (6)$$

where  $a > 0$  and  $b > 0$  are parameters and  $L^*$  is a scaling factor (below taken equal 1 km in order to keep expression in brackets dimensionless). From Eq. 6 and condition  $r(L_0) = 1$  we can estimate scale  $L_0$ , which can be understood as a scale of rigidity.

The ice velocities at the ADCP site and those estimated by drifters for ice periods C, D and E were well correlated in space (Table 3). Only

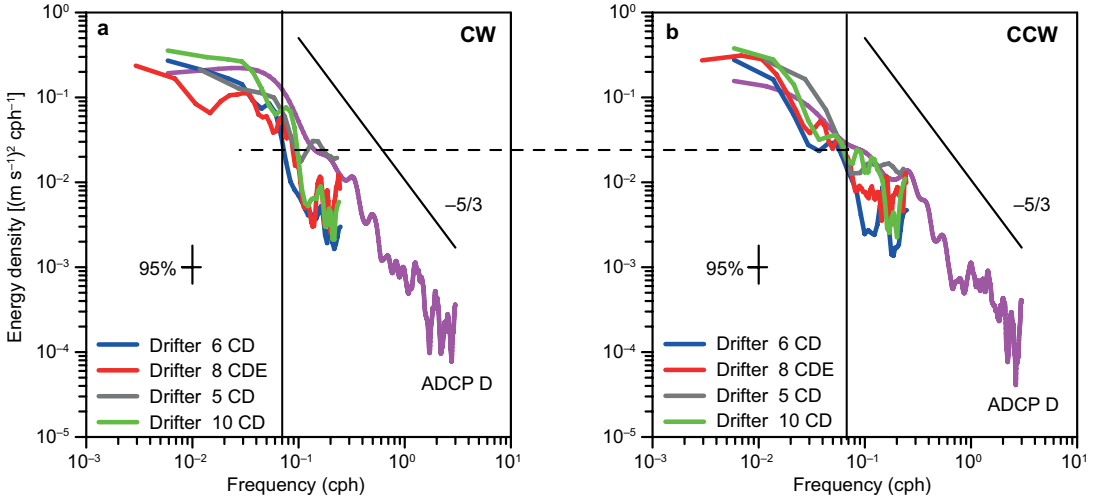


**Fig. 12.** Ice velocity spectra at the drifters. CW is for clockwise and CCW for counter-clockwise frequencies. Vertical thin line marks inertial frequency; the horizontal dashed line helps to compare energy densities at the inertial frequency for CW and CCW spectra. The inclined solid line refers to spectral slope  $-5/3$ . For comparison, the ADCP period D spectra are given.

in two cases, the correlation was not significant ( $p > 0.05$ ). The best fit for Eq. 6 resulted in  $a = 0.91$  and  $b = 0.18$ , when the scaling factor was selected as  $L^* = 1$  km (Fig. 13). The scatter was, however, fairly large. Using the best-fit parameters, the correlation becomes one at  $L_0 = 0.7$  km,

**Table 3.** Covariance/correlation matrix of ADCP and drifter velocities for ice periods C, D and E. Italic marks not significant correlation ( $p > 0.05$ ). Numbers in parentheses are the representative distances (km) for correlation calculations between drifters and ADCP site and between different drifters.

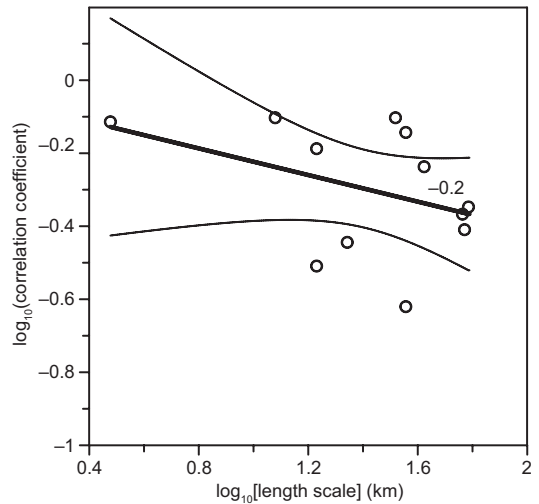
C	ADCP	Drifter 5	Drifter 6
ADCP	331.5	207.8	257.9
Drifter 5	0.79 (33)	206.7	221.6
Drifter 6	0.72 (36)	0.79 (12)	379.5

D	ADCP	Drifter 6	Drifter 8	Drifter 10
ADCP	201.8	24.6	70.9	75.3
Drifter 6	0.24 (36)	49.4	25.6	34.4
Drifter 8	0.43 (58)	0.31 (17)	131.9	120.8
Drifter 10	0.39 (59)	0.36 (22)	0.77 (3)	182.9

E	ADCP	Drifter 6	Drifter 8
ADCP	441.1	130.7	93.1
Drifter 6	0.58 (42)	116.2	69.2
Drifter 8	0.45 (61)	0.65 (17)	96.5



**Fig. 13.** Spatial correlation of ice velocity as a function of length scale. The solid line  $-0.2$  is the best fit line and the thin lines show its 95% confidence limits.

which corresponds to the scale of the size of ice floes. The distance where the spatial correlation had decreased to 0.5 was 28 km. We also determined the integral length scale as the e-folding scale of correlation, resulting in 48 km. This also scales with the width of the basin, therefore, the basin boundaries influence all over the drift ice field.

## Summary and conclusions

The drift of sea ice in the Baltic Sea is a key issue in ensuring the safety of winter navigation and estimating loads on fixed structures. The size of the Baltic Sea basins is of the order of the length scale of sea ice stress when the internal friction and consequently ice concentration is high. Therefore, the fixed boundaries are felt everywhere in the presence of high ice compactness and the ice field may be stationary. For open ice fields, internal stresses are negligible and the free drift state is realizable. Earlier field investigations of ice dynamics in the Baltic Sea were based on surface drifters and SAR satellite data over 1–2 week periods (Leppäranta 1981, Leppäranta *et al.* 1998, 2001, Uotila 2001). In these studies, the wind factor in sea ice drift, as well as the strain-rate and vorticity fields, were examined. More recently, longer-term ice drift measurements were conducted in the Baltic Sea in winter season 2004 at an ADCP site (Björk *et al.* 2008). This work is an extension of the earlier studies since we have relatively large spatial coverage by drifters and high-frequency temporal coverage at one site by ADCP.

Sea ice kinematics provides the deformation fields and forms the basis for the development of ice stress fields. Wind is the main force to build strong ice compression. The Gulf of Finland is tailored to the development of ice compression in the case of along-gulf, westerly winds due to its elongated shape and fixed boundary in the east. The sea area off Kunda, in the middle of the Gulf of Finland, is known for severe ice conditions and, therefore, was selected for the ADCP measurements to study local high-resolution ice kinematics. The spatial coverage of measurements was achieved by deploying drifters in two groups further north from the ADCP site. The MODIS satellite images allowed to validate the ADCP ability to detect ice cover versus open waters and to conclude that the latter is a reliable tool for the sea ice drift measurements.

Here, we focused on the ice drift character in the Gulf of Finland relying on the combined *in situ* and remote sensing measurement technology. We concentrated on scales of 10 to 60 km to understand how the sea ice velocity behaves at the spatial scales smaller than the basin scale.

The analysis of experiment data revealed frequent alternations between the ice cover periods and open water periods in the Gulf of Finland. Leads were present near the northern and southern coasts due to frequent changes in wind direction. A total of five ice periods with a duration of 6–12 days were obtained in the measurement region over a total duration of about two and half months (periods A, B, C, D, and E). In period C, three instruments (buoy 5, buoy 6 and the ADCP) showed a coincident ice drift direction, indicating uniform ice drift in the middle of the Gulf of Finland. Ice movement was correlated with wind data measured nearby. The mean asymptotic wind factor at large wind speeds was 0.034, corresponding to the ratio of 0.92 of the air–ice and water–ice drag coefficients. The Ekman angle was  $9^\circ$  in the oceanic boundary layer. Both parameters were affected by the geometry of the Gulf of Finland. Namely, in the cases when the wind was pushing ice eastward, the wind factor was below the mean value and when the wind was in opposite direction, the wind factor was above the mean. The asymptotic wind factor and its dependence on the wind direction were in accordance with a study performed in the northern part of the Bothnian Bay. Leppäranta (1981) obtained there the asymptotic wind factor of 0.026, while Björk *et al.* (2008) found a value of about 0.03 that decreased due to the long-term southerly and easterly winds to 0.01–0.02 as ice stresses became dominant. Therefore, implementing the classical purely wind-driven free drift model of ice in the Gulf of Finland, the wind direction dependence of wind factor and deviation angle has to be considered.

Ice drift was mostly in near-free drift state driven by winds and, at times, also by ice-independent currents in the basin. The ice velocity clockwise spectra (both Eulerian (ADCP) and Lagrangian (drifters)) showed an elevated level around the inertial frequency and a power law by exponent  $-1.8$  in the higher frequencies. Eulerian clockwise spectra showed a higher level than the Lagrangian spectra in the frequencies of 0.04–0.2 cph. Eulerian and Lagrangian counter-clockwise spectra had roughly the same energy density values. Thus both types of measurements confirmed the contribution of inertial oscillations to the ice drift velocity field. These results

are most useful for constructing local short-term forecasting systems for ice drift, e.g., at access to harbours. Spatial correlations were significant in the range from 3 to 60 km, with the best-fit falling power of  $-0.18$ . The correlation level approached 1 at about 1 km distance (i.e., at the scale of the size of ice floes, although the scatter of the correlation vs. length scale was large). The estimated integral correlation length scale was 48 km. As this scales with the width of the basin, the boundaries of the basin influence all over the drift ice field. The spatial correlation structure provides useful information for controlling ship channels and evaluating ice forces.

*Acknowledgments:* Preliminary results were obtained within the FP7 EU-funded project “Safety of winter navigation in dynamic ice” (contract SCP8-GA-2009-233884 – SAFEWIN). Later on, the study was partly supported by Estonian Science Foundation grant no. ETF9381 and by institutional research funding (IUT19-6) of the Estonian Ministry of Education and Research. We are grateful to the crew and the scientific team of the R/V *Aranda* led by Dr. Jari Haapala, for assistance in the deployment of the drifting buoys and to Kaimo Vahter for the assistance in drifter data processing. The authors thank NASA’s Goddard Space Flight Center for providing MODIS data and E.U. Copernicus Marine Service Information for providing sea ice concentration data. Special thanks go to Liis Sipilgas and Ove Pärn who processed the MODIS and ice concentration data respectively. Also, we thank anonymous reviewers for their helpful comments.

## References

- Alenius P., Myrberg K. & Nekrasov A. 1998. The physical oceanography of the Gulf of Finland: a review. *Boreal Env. Res.* 3: 97–125.
- Belliveau D.J., Bugden G.L., Eid B.M. & Calnan C.J. 1990. Sea ice velocity measurements by upward-looking Doppler current profilers. *J. Atmos. Oceanic Technol.* 7: 596–602.
- Björk G., Nohr C., Gustafsson B.G. & Lindberg A.E.B. 2008. Ice dynamics in the Bothnian Bay inferred from ADCP measurements. *Tellus* 60A: 178–188.
- Girard L., Weiss J., Molines J.M., Barnier & Bouillon B. 2009. Evaluation of high-resolution sea ice models on the basis of statistical and scaling properties of Arctic sea ice drift and deformation. *Journal of Geophysical Research: Oceans* 114(C8), doi:10.1029/2008JC005182.
- Goldstein R.V., Osipenko N.M. & Leppäranta M. 2009. Relaxation scales and the structure of fractures in the dynamics of sea ice. *Cold Regions Science and Technology* 58: 29–35.
- Hibler W.D.III 1986. Ice dynamics. In: Untersteiner N. (ed.), *Geophysics of Sea Ice*, Plenum Press, New York, pp. 577–640.
- Hibler W.D.III, Weeks W.F., Kovacs A. & Ackley S.F. 1974. Differential sea-ice drift. I. Spatial and temporal variations in sea ice deformation. *Journal of Glaciology* 13: 437–455.
- Joffre S.M. 1982. Momentum and heat transfer in the surface layer over a frozen sea. *Boundary-Layer Meteorology* 24: 211–229.
- Kheysin D.Ye. 1978. Relationship between mean stresses and local values of internal forces in a drifting ice cover. *Oceanology* 18: 285–286.
- Kõuts T., Pavelson J. & Lilover M.-J. 2012. *Monitoring of ice dynamics using bottom-mounted ADCP in the central Gulf of Finland in 2010*. Baltic International Symposium (BALTIC), 2012 IEEE/OES, doi:10.1109/BALTIC.2012.6249179.
- Kundu P.K. 1976. Ekman veering observed near the ocean bottom. *J. Phys. Oceanogr.* 6: 238–242.
- Leppäranta M. 1981. On the structure and mechanics of pack ice in the Bothnian Bay. *Finnish Mar Res.* 248: 3–86.
- Leppäranta M. 2011. *The drift of sea ice*, 2nd ed. Springer-Verlag, Berlin-Heidelberg.
- Leppäranta M. & Hakala R. 1992. The structure and strength of first-year ice ridges in the Baltic Sea. *Cold Regions Sci. Technol.* 20: 295–311.
- Leppäranta M. & Omstedt A. 1990. Dynamic coupling of sea ice and water for ice field with free boundaries. *Tellus* 42A: 482–495.
- Leppäranta M., Sun Y. & Haapala J. 1998. Comparison of sea ice velocity fields from ERS-1 SAR and dynamic model. *J. Glaciol.* 44: 248–262.
- Leppäranta M., Zhang Z., Haapala J. & Stipa T. 2001. Sea ice mechanics in a coastal zone of the Baltic Sea. *Annals of Glaciology* 33: 151–156.
- Leppäranta M., Oikkonen A., Shirasawa K. & Fukamachi Y. 2012. A treatise on frequency spectrum of drift ice velocity. *Cold Regions Science and Technology* 76–77: 83–91.
- Lilover M.-J., Pavelson J. & Kõuts T. 2013. High resolution ice dynamics derived from ADCP and icebound drifter data in the Gulf of Finland, Baltic Sea. In: *Proceedings of the 22nd International Conference on Port and Ocean Engineering under Arctic Conditions, June 9–13, 2013, Espoo, Finland*, pp. 1414–1425.
- Lips U., Laanemets J., Lips I., Liblik T., Suhhova I. & Suursaar Ü. 2017. Wind-driven residual circulation and related oxygen and nutrient dynamics in the Gulf of Finland (Baltic Sea) in winter. *Estuarine Coastal and Shelf Science* 195: 4–15.
- MacMahan J., Brown J. & Thornton E. 2009. Low-cost handheld global positioning system for measuring surf-zone currents. *Journal of Coastal Research* 25: 744–754.
- Ono N. 1978. Inertial period motions of drifting ice. *Low Temperature Science* A37: 107–113.
- Overland J.E., Walter B.A., Curtin T.B. & Turet P. 1995. Hierarchy in sea ice mechanics: a case study from the Beaufort Sea. *Journal of Geophysical Research* 100(C3): 4559–4571.
- Pärn O. & Haapala J. 2011. Occurrence of synoptic flaw leads of sea ice in the Gulf of Finland. *Boreal Env. Res.*

- 16: 71–78.
- Richter-Menge J., McNutt S.L., Overland J.E. & Kwok R. 2002. Relating arctic pack ice stress and deformation under winter conditions. *Journal of Geophysical Research* 107(C10), doi:10.1029/2000JC000477.
- Ryabchenko V., Dvornikov A., Haapala J. & Myrberg K. 2010. Modelling ice conditions in the easternmost Gulf of Finland in the Baltic Sea. *Continental Shelf Research* 30: 1458–1471.
- Sanderson T.J.O. 1988. *Ice mechanics. Risks to Offshore Structures*. Graham & Trotman, Boston.
- Shevchenko G.V., Rabinovich A.B. & Thomson R.E. 2004. Sea-ice drift on the northeastern shelf of Sakhalin Island. *Journal of Physical Oceanography* 34: 2470–2491.
- Shcherbina A.Y., Rudnick D.L. & Talley L.D. 2005. Ice-draft profiling from bottom-mounted ADCP data. *J. Atmos. Oceanic Technol.* 22: 1249–1266.
- Soomere T. 2003. Anisotropy of wind and wave regimes in the Baltic Proper. *J. Sea Res.* 49: 305–316.
- Soomere T., Myrberg K., Leppäranta M. & Nekrasov A. 2008. Progress in physical oceanography of the Gulf of Finland, Baltic Sea. *Oceanologia* 50: 287–362.
- Stern H.L. & Lindsay R.W. 2009. Spatial scaling of Arctic sea ice deformation. *Journal of Geophysical Research: Oceans* 114(C10), doi:10.1029/2009JC005380.
- Strass V. 1998. Measuring sea ice draft and coverage with upward-looking moored sonar. *Deep-Sea Res.* 45: 795–818.
- Thorndike A.S. 1986. Kinematics of sea ice. In: Untersteiner N. (ed.), *Geophysics of sea ice*, Plenum Press, New York, pp. 489–549.
- Thorndike A.S. & Colony R. 1982. Sea ice motion in response to geostrophic wind. *J. Geophys. Res.* 87(C8): 5845–5852.
- Uotila J. 2001. Observed and modelled sea-ice drift response to wind forcing in the northern Baltic Sea. *Tellus* 53A: 112–128.
- Visbeck M. & Fischer J. 1995. Sea surface conditions remotely sensed by upward-looking ADCPs. *J. Atmos. Oceanic Technol.* 12: 141–149.
- Weiss J. 2013. *Drift, Deformation and Fracture of Sea Ice — A Perspective Across Scales*. Springer, Netherlands.